Hindawi
Mathematical Problems in Engineering
Volume 2019, Article ID 1631930, 17 pages
https://doi.org/10.1155/2019/1631930

Research Article

Maneuverability Analysis of a Novel Portable Modular AUV

Xiaoming Wang and Shengguo Liang

School of Mechanical Engineering, Tianjin University of Science and Technology, Tianjin 300222, China

Correspondence should be addressed to Xiaoming Wang; wxm@tust.edu.cn

Received 19 February 2019; Revised 5 May 2019; Accepted 3 June 2019; Published 26 June 2019

Academic Editor: Boulaïd Boulkroune

ZFAUV is a novel portable modular AUV. There are four fixed thrusters at tail, and two tunnel thrusters are set at front. The maneuverability of ZFAUV is relatively high. It can turn around in situ, move lateral or move up/down vertical. The yaw and pitch can be controlled by tunnel thrusters or differential control of tail thrusters, but differential control will reduce the forward force. Different from propeller-rudder AUVs, the turning radius is related to speed forward: the smaller the speed forward, the smaller the turning radius. The minimum turning radius tends to be zero. The mathematical model is built first; then CFD is used to predict the thrust and torque of tail thrusters and tunnel thrusters. Through numerical simulation, zigzag maneuver analysis in horizontal plane, and trapezoidal steering maneuver analysis in vertical plane, the maneuverability of ZFAUV is obtained. The maneuverability of ZFAUV becomes worse with the increase of speed. The maneuverability of differential control is better than that of tunnel control. In the case of specific thrust distribution of tail thrusters and tunnel thrusters, ZFAUV can turn around in situ (the maximum angular velocity is about 24.1°/s), move lateral or move up/down vertical (the maximum velocity is about 0.4m/s). Finally, an example, PID parameters tuning, is given to illustrate the application of maneuverability analysis. The dynamic performance of ZFAUV can be quickly and accurately analyzed by mathematical method, which has important guiding significance for the choice of control strategy and experiments and also has reference value for the later development of AUVs.

1. Introduction

Autonomous Underwater Vehicle (AUV) is defined as a vehicle that can perform underwater tasks and missions autonomously, using onboard navigation, guidance, and control systems [1]. AUVs are being used increasingly in a variety of applications, such as surveys, exploration, inspection, maintenance and construction, search and rescue, environmental and biological monitoring, military, undersea mining, and recreation [2].

Due to the limitation of weight and economic cost, most AUVs use fewer thrusters to achieve multi-degree-of-freedom coupling motion control, which makes them typical underactuated system. The shape of these AUVs is generally streamlined, most are torpedo-shaped (e.g., the NERC Autosub6000 AUV and REMUS-100 AUV). The traditional propeller-rudder control mode is adopted by most AUVs that is a main propeller and control surface is arranged at the tail. At present, the control systems adopted by underactuated AUVs are generally classified into the following categories: X rudder[3], cross rudder[4, 5], rudder behind propeller[6], and rudder at front [2]. But the rudder efficiency is relatively low at low speed, the steering force is greatly reduced, and the mobility is insufficient. In order to improve the maneuverability at low speed, through-body tunnel thrusters were adopted [7], some researchers have put forward vector propulsion system instead of the traditional propeller-rudder control system [8], and some have a more complex configuration allowing them to move more slowly and across complex terrain, e.g., the WHOI ABE and SENTRY AUVs [9]. There are many problems for the control surfaces mentioned above, such as the driving mechanism is complex, maintenance is more difficult, and so on. The adoption of differential control of multiple fixed thrusters can avoid these problems; the horizontal and vertical motions are just adjusted by the speed of thrusters, e.g., X4AUV [10–15], but X4AUV is only a model at present and has no practical application.

We developed a small portable modular AUV with four fixed thrusters at tail, named ZFAUV; it weighs about 20kg. Meanwhile, in order to improve the maneuverability of

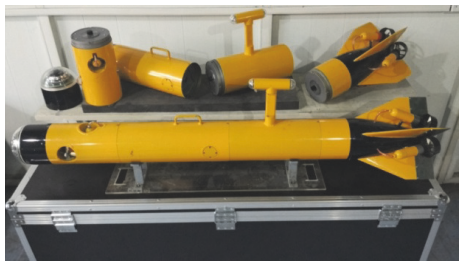

Figure 1: Modular ZFAUV.

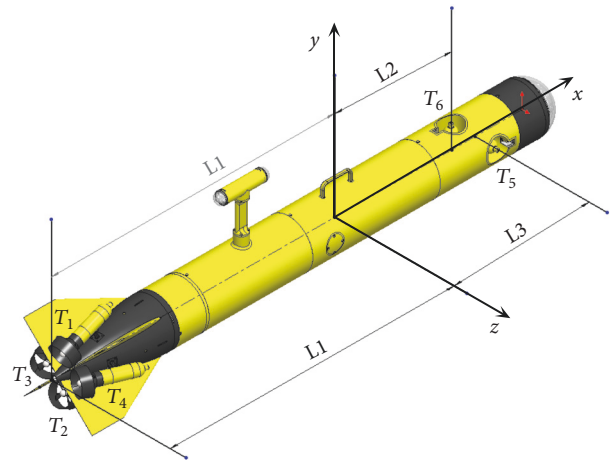

Figure 2: Thruster arrangement.

ZFAUV, two tunnel thrusters are set at front: one is horizontal and the other is vertical, as shown in Figure 1. With the aid of these six thrusters, some actions that ordinary propeller-rudder AUVs cannot achieve, such as turning around in situ, moving lateral, moving up/down vertical, etc., can be achieved.

To the best of our knowledge, the AUVs who have tunnel thrusters both at front and at rear are both conventional propeller-rudder AUVs. They are equipped with two tunnel thrusters (vertical usually) [16] or four tunnel thrusters (two horizontal and two vertical) [17, 18]. The purpose is to improve the maneuverability at low speed, achieve near-bottom and low-speed sailing, moving up/down vertical, etc. But in order to achieve turning around in situ, moving lateral, moving up/down vertical etc., four tunnel thrusters are needed at least; this is difficult for small AUV due to the limited space. For the speed of the tail thrusters of ZFAUV can be different, or even reversed, the effect is the same as that of vertical and horizontal tunnel thrusters at rear. So the limited space can be used to equip other sensors.

Researchers model the dynamic behavior of AUVs to evaluate their performances [19]. The turning circle and spiral and zigzag maneuvers are usually designed and used to evaluate the performance of AUVs [20, 21]. Kim et al. used spiral and zigzag maneuvers to model linear AUV system [22].

Mathematical model is needed to predict the maneuverability; although numerous underwater vehicle models have been presented, there is a little study of the model of this novel AUV with four fixed thrusters and two tunnel thrusters. Thus, there is an urgent need to build dynamics model for this novel AUV. Meanwhile, there are many hydrodynamic coefficients in the mathematical model. Generally, there are two different approaches to obtain the hydrodynamic coefficients. The conventional method is towing tank experiment, but it takes a long time and costs a lot. The other method is using of CFD. In the field of AUVs, the use of CFD has increased in recent years due to the increasing availability of powerful computers and user-friendly CFD software, which has become an almost completely necessary tool for predicting the hydrodynamic coefficients used in maneuverability predictions [23]. And advances on high-performance computing brought the possibility of numerically solving differential equations with high degree of difficulty [24].

The purpose of this study is to simulate the maneuverability of ZFAUV. So the mathematical model is built first; then the CFD is used to predict the thrust and torque of thrusters. And the mathematical model is simplified in horizontal plane and vertical plane, respectively. The motion characteristics of ZFAUV are studied in detail, including steady linear maneuver, maneuverability in vertical plane, maneuverability in horizontal plane, etc.

The rest of this paper is organized as follows. Section 2 presents the mathematical model. The thrust and torque of tail thrusters and tunnel thrusters is calculated with CFD in Section 3. In Section 4, motion simulation and maneuverability analysis is offered. An example, PID parameters tuning, is given to illustrate the application of maneuverability analysis in Section 5. Section 6 concludes the paper.

2. Mathematical Model

2.1. Geometric Model. As shown in Figure 1, ZFAUV with four fixed thrusters at tail and two tunnel thrusters at front is proposed in this paper. The thrusters' number is shown in Figure 2. T_5 is horizontal tunnel thruster, T_6 is vertical tunnel thruster, T_1 and T_2 are vertical thrusters, and T_3 and T_4 are horizontal thrusters. The angle between T_1, T_2, T_3, T_4 and Ox axis is ϑ, $\vartheta = 22.5^\circ$.

2.2. Motion Analysis. The forces and torques acting on ZFAUV are complex during the survey task, including gravity, buoyancy, thruster's thrust, and water resistance. In order to study the motion of ZFAUV, we only analyze the influence of thruster's thrust on the attitude of ZFAUV.

Figures 3(a)–3(i) are the top view of ZFAUV. For the thrust of thruster is adjustable, the following is a simple analysis of the situation of $|T_3| = |T_4|$ and $T_1 = T_2 > 0$.

Figure 3(a), $T_3 = T_4 > 0$, $T_5 = 0$, ZFAUV moves forward.

Figure 3(b), $T_3 = T_4 > 0$, $T_5 > 0$, ZFAUV turns right.

Figure 3(c), $T_3 = -T_4 > 0$, $T_5 = 0$, ZFAUV turns right.

Figure 3(d), $T_3 = T_4 > 0$, $T_5 < 0$, ZFAUV turns left.

Figure 3(e), $T_3 = -T_4 < 0$, $T_5 = 0$, ZFAUV turns left.

Figure 3(f), $T_3 = -T_4 < 0$, $T_5 > 0$, ZFAUV can move right lateral under certain conditions.

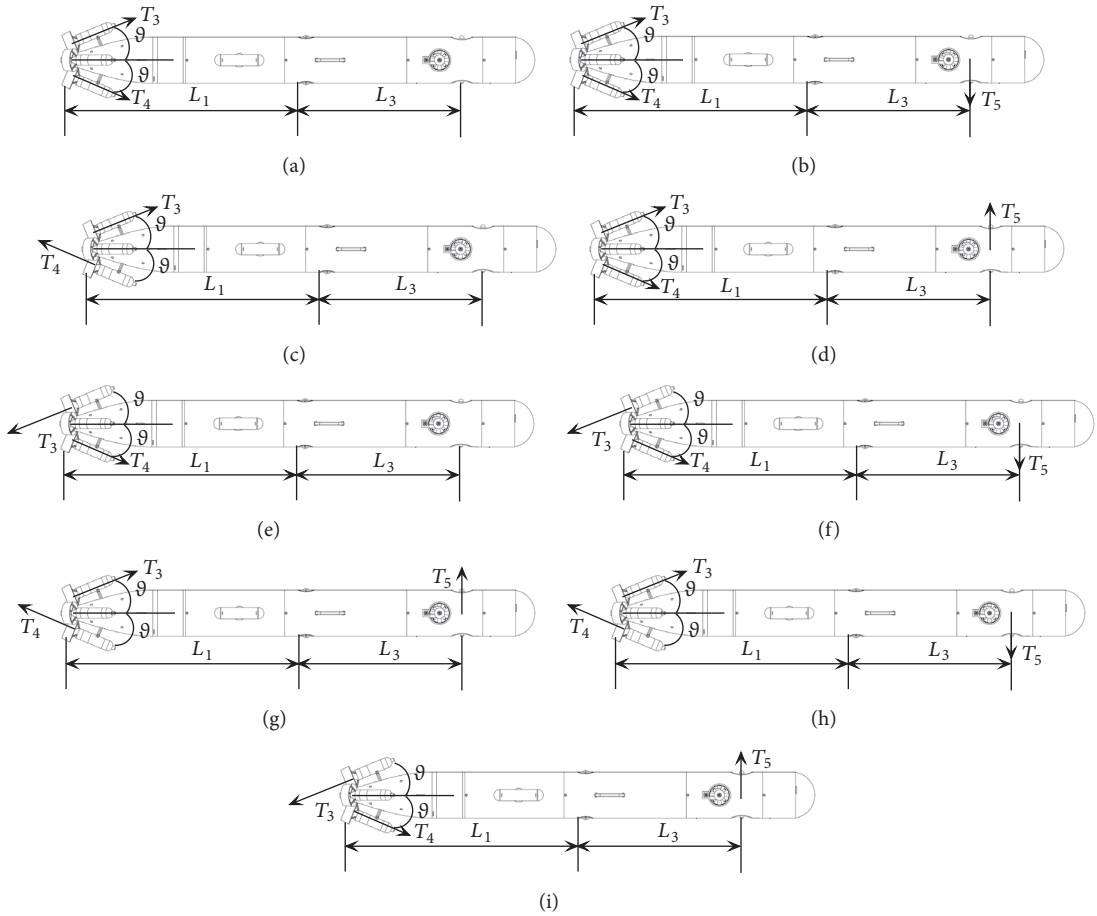

Figure 3: Motion of ZFAUV in horizontal plane.

Figure 3(g), $T_3 = -T_4 > 0$, $T_5 < 0$, ZFAUV can move left lateral under certain conditions.

Figure 3(h), $T_3 = -T_4 > 0$, $T_5 > 0$, ZFAUV can turn right in situ under certain conditions.

Figure 3(i), $T_3 = -T_4 < 0$, $T_5 < 0$, ZFAUV can turn left in situ under certain conditions.

In the case of differential control, Figures 3(c) and 3(e), ZFAUV can turn right or left, but the forward force will decrease. So, the yaw is better to be controlled by the tunnel thruster.

Figures 4(a)–4(g) are the side view of ZFAUV; the following is a simple analysis of the situation of $|T_1| = |T_2|$ and $T_3 = T_4 > 0$.

Figure 4(a), $T_1 = T_2 > 0$, $T_6 = 0$, ZFAUV moves forward.

Figure 4(b), $T_1 = T_2 > 0$, $T_6 < 0$, ZFAUV turns down.

Figure 4(c), $T_1 = -T_2 > 0$, $T_6 = 0$, ZFAUV turns down.

Figure 4(d), $T_1 = T_2 > 0$, $T_6 > 0$, ZFAUV turns up.

Figure 4(e), $T_1 = -T_2 < 0$, $T_6 = 0$, ZFAUV turns up.

Figure 4(f), $T_1 = -T_2 < 0$, $T_6 < 0$, ZFAUV can move down vertical under certain conditions.

Figure 4(g), $T_1 = -T_2 > 0$, $T_6 > 0$, ZFAUV can move up vertical under certain conditions.

In the case of differential control, Figures 4(c) and 4(e), ZFAUV can turn up or down, but the forward force will decrease also. So, the pitch is better to be controlled by the tunnel thruster.

2.3. Reference Frames. In order to model ZFAUV, two reference frames are defined to describe motion of ZFAUV: the body-fixed reference frame ($B - xyz$) and the earth-fixed reference frame ($E - XYZ$). Figure 5 shows the reference frames.

2.4. Kinematics and Dynamics. According to reference (Fossen, 2011; Xiaoming Wang, 2009)[25, 26], we design the kinematics and dynamics equations. They are shown separately as

$$\dot{\varphi} = p - (q\cos\varphi - r\sin\varphi)\tan\theta$$

$$\dot{\theta} = q\sin\varphi + r\cos\varphi$$

$$\dot{\psi} = \frac{(q\cos\varphi - r\sin\varphi)}{\cos\theta}$$

$$\dot{X}_e = u\cos\theta\cos\psi + v(\sin\psi\sin\varphi - \sin\theta\cos\psi\cos\varphi) + w(\sin\psi\cos\varphi + \sin\theta\cos\psi\sin\varphi)$$

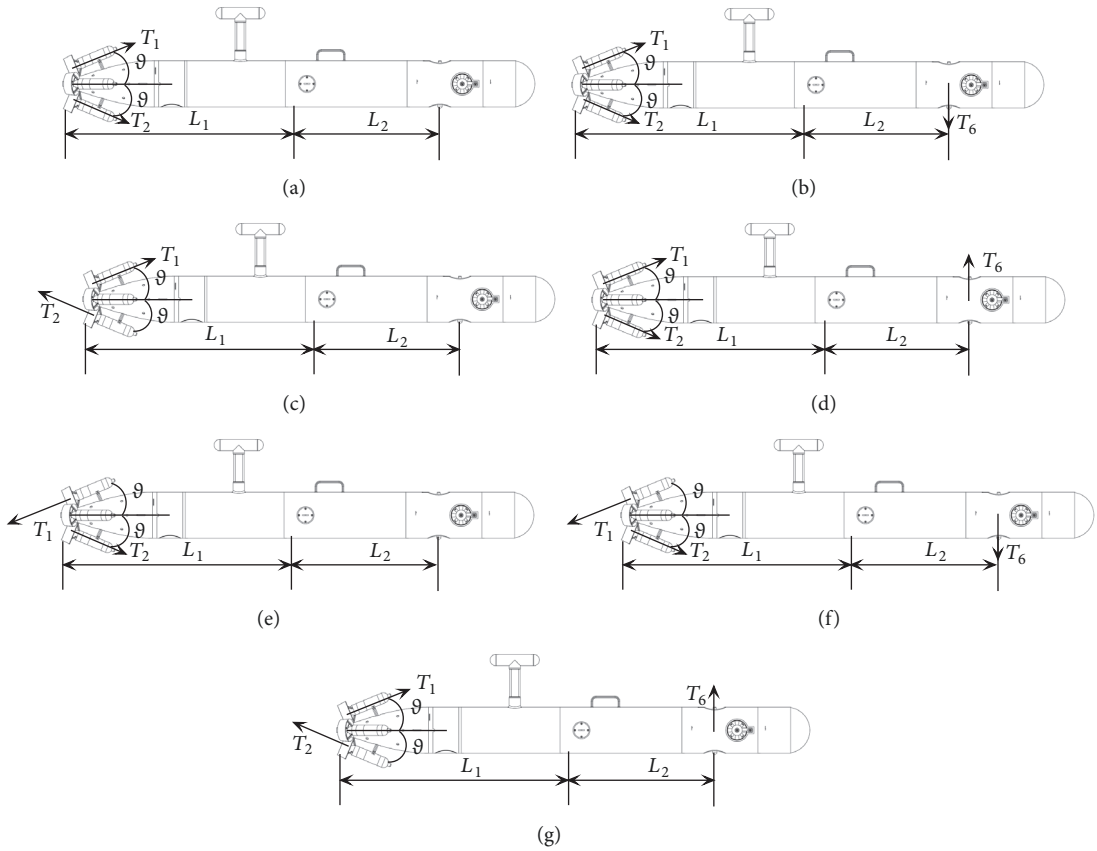

Figure 4: Motion of ZFAUV in vertical plane.

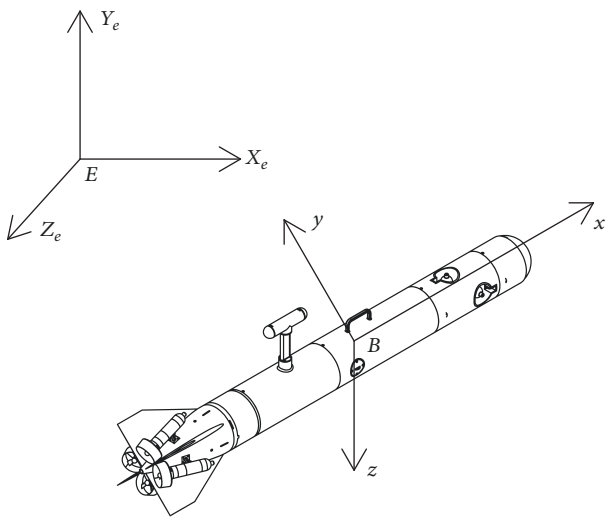

Figure 5: Reference frame of ZFAUV.

$$
\begin{aligned}
&\dot{Y}_e = u\sin\theta + v\cos\theta\cos\varphi - w\cos\theta\sin\varphi\\
&\dot{Z}_e\\
&\quad = -u\cos\theta\sin\psi\\
&\qquad + v\left(\cos\psi\sin\varphi + \sin\theta\sin\psi\cos\varphi\right)\\
&\qquad + w\left(\cos\psi\cos\varphi - \sin\theta\sin\psi\sin\varphi\right)\\
&V_T = \sqrt{u^2 + v^2 + w^2}\\
&\alpha = \arctan\left(-\frac{v}{u}\right)\\
&\beta = \arcsin\left(\frac{w}{V_T}\right)
\end{aligned}
\tag{1}
$$

$$
\begin{aligned}
&\left(m + \lambda_{11}\right)\dot{u}\\
&\quad = mvr - \Delta G\sin\theta + \left(T_1 + T_2 + T_3 + T_4\right)\cos\vartheta\\
&\qquad + \frac{1}{2}\rho V^2{}_T S C_x\left(0\right)\\
&\left(m + \lambda_{22}\right)\dot{v} + \lambda_{26}\dot{r}\\
&\quad = -mur - \Delta G\cos\theta\cos\varphi + \left(T_1 - T_2\right)\sin\vartheta + T_6\\
&\qquad + \frac{1}{2}\rho V^2{}_T S\left(C_Y^{\alpha}\alpha + C_Y^{r}r'\right)\\
&\left(m + \lambda_{33}\right)\dot{w} + \lambda_{35}\dot{q}\\
&\quad = muq + \Delta G\cos\theta\sin\varphi
\end{aligned}
$$

$$
\begin{aligned}
&+\frac{1}{2}\rho V^2{}_T S\left(C_Z^\beta\beta+C_Z^p p'+C_Z^q q'\right)+T_5\\
&-\left(T_3-T_4\right)\sin\vartheta\\
&\left(J_x+\lambda_{44}\right)\dot{p}\\
&=my_G uq+Gy_G\cos\theta\sin\varphi\\
&+\frac{1}{2}\rho V^2{}_T SL\left(C_R^\beta\beta+C_R^p p'+C_R^q q'\right)\\
&+\left(-Q_1+Q_2-Q_3+Q_4\right)\cos\vartheta\\
&\left(J_y+\lambda_{55}\right)\dot{q}+\lambda_{35}\dot{w}\\
&=\frac{1}{2}\rho V^2{}_T SL\left(C_M^\beta\beta+C_M^p p'+C_M^q q'\right)\\
&-\left(T_3-T_4\right)\sin\vartheta L_1-T_5L_3+\left(-Q_1+Q_2\right)\sin\vartheta\\
&+Q_6\\
&\left(J_z+\lambda_{66}\right)\dot{r}+\lambda_{26}\dot{v}\\
&=Gy_G\sin\theta+\frac{1}{2}\rho V^2{}_T SL\left(C_N^\alpha\alpha+C_N^r r'\right)\\
&-\left(T_1-T_2\right)\sin\vartheta L_1+T_6L_2+\left(Q_3-Q_4\right)\sin\vartheta\\
&+Q_5
\end{aligned}
\tag{2}
$$

where

$$
\begin{aligned}
T_1&=\frac{K_{T1}\rho {D_1}^4}{60^2}n_1\left|n_1\right|n_{\max1}^2\\
T_2&=\frac{K_{T1}\rho {D_1}^4}{60^2}n_2\left|n_2\right|n_{\max2}^2\\
T_3&=\frac{K_{T1}\rho {D_1}^4}{60^2}n_3\left|n_3\right|n_{\max3}^2\\
T_4&=\frac{K_{T1}\rho {D_1}^4}{60^2}n_4\left|n_4\right|n_{\max4}^2\\
T_5&=\frac{K_{T2}\rho {D_2}^4}{60^2}n_5\left|n_5\right|n_{\max5}^2\\
T_6&=\frac{K_{T2}\rho {D_2}^4}{60^2}n_6\left|n_6\right|n_{\max6}^2,\\
Q_1&=\frac{K_{Q1}\rho {D_1}^5}{60^2}n_1\left|n_1\right|n_{\max1}^2\\
Q_2&=\frac{K_{Q1}\rho {D_1}^5}{60^2}n_2\left|n_2\right|n_{\max2}^2\\
Q_3&=\frac{K_{Q1}\rho {D_1}^5}{60^2}n_3\left|n_3\right|n_{\max3}^2\\
Q_4&=\frac{K_{Q1}\rho {D_1}^5}{60^2}n_4\left|n_4\right|n_{\max4}^2\\
Q_5&=\frac{K_{Q2}\rho {D_2}^5}{60^2}n_5\left|n_5\right|n_{\max5}^2\\
Q_6&=\frac{K_{Q2}\rho {D_2}^5}{60^2}n_6\left|n_6\right|n_{\max6}^2,\\
p'&=\frac{pL}{V_T},\\
q'&=\frac{qL}{V_T},\\
r'&=\frac{rL}{V_T},
\end{aligned}
\tag{3}
$$

(X_e, Y_e, Z_e) is the position in E, φ, θ, and ψ are roll angle, pitch angle, and yaw angle, and p, q, and r are the angular velocity.

Some physical parameters in the model, such as m, D_1, D_2, J_x, J_y, J_z, etc., can be acquired by 3D modeling software (SolidWorks). Other hydrodynamic coefficients (for example, K_T and K_Q of thrusters in Section 3) can be obtained by CFD simulation.

3. Thrust Analysis

For ZFAUV, the power comes from each thruster. Therefore, the performance of thruster is very important for the dynamic performance and maneuverability of ZFAUV. Therefore, the thrust of tail thruster and tunnel thruster under different conditions needs to be analyzed in detail.

Thrust performance analysis of thruster is relatively complex. There are two main ways at present. First, physical test, the results are accurate, but the cycle is long, which requires a huge amount of manpower and material resources. Second, CFD simulation, with low cost and short cycle, can obtain complete data and can set up computational flow field according to research needs, which is sometimes difficult to achieve in physical experiments. Therefore, CFD method is used to predict the thrust.

In the numerical calculation, the propeller is assumed to be located deep below the water surface, without considering the influence of surface effects such as surface waves. In order to simulate the infinite flow field, the size of computational domain should be much larger than 10 times the diameter of the propeller to ensure that the boundary layer has no effect on the motion of the propeller. According to the characteristics of propeller when it rotates, the computational domain is divided into two parts: the dynamic region near the propeller and the static region far from the propeller, as shown in Figures 6 and 7. Multiple reference frames (MRF) method is used; that is, the rotating coordinate system is used to solve the dynamic fluid-1 and the Cartesian inertial coordinate system is used to solve the static fluid-2.

Three-dimensional solver in Fluent is used to solve the physical model, and unsteady uncoupled invisible algorithm is used. Modified RNG k-ε turbulence equation is used to describe the turbulence model, and enhanced wall function is used to solve the flow around the wall. The pressure-velocity

Table 1: Calculated thrust and torque of tail thruster at different flow velocity.

T/N Q/N•m	n/%					
	10	20	40	60	80	100
v_{flow}/m/s						
0.26	1.47	3.31	5.89	12.95	22.82	35.41
	0.0173	0.0403	0.0714	0.1596	0.2815	0.4391
0.56	1.17	2.78	5.06	11.59	20.71	32.43
	0.0161	0.0381	0.0674	0.1538	0.2725	0.4249
1.14	0.82	2.24	4.40	10.26	18.51	25.76
	0.0119	0.0316	0.0605	0.1401	0.2519	0.3935
1.79	0.48	1.69	3.68	8.93	16.46	20.39
	0.0060	0.0223	0.0481	0.1198	0.2194	0.3560
2.22	0.13	1.13	3.03	7.60	14.26	14.42
	0.0018	0.0159	0.0412	0.1061	0.1988	0.3267
2.87	-0.22	0.57	2.37	6.27	12.06	8.46
	-0.0024	0.0094	0.0343	0.0923	0.1782	0.2975

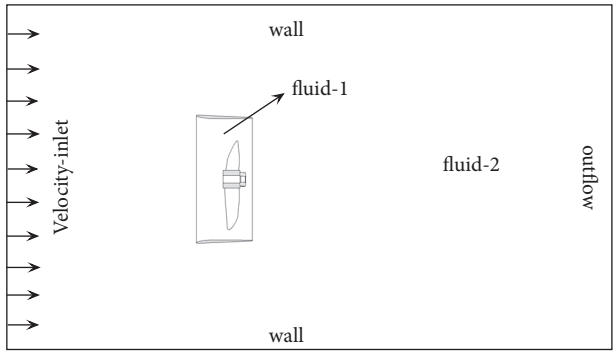

Figure 6: Physical model of tail thruster in CFD.

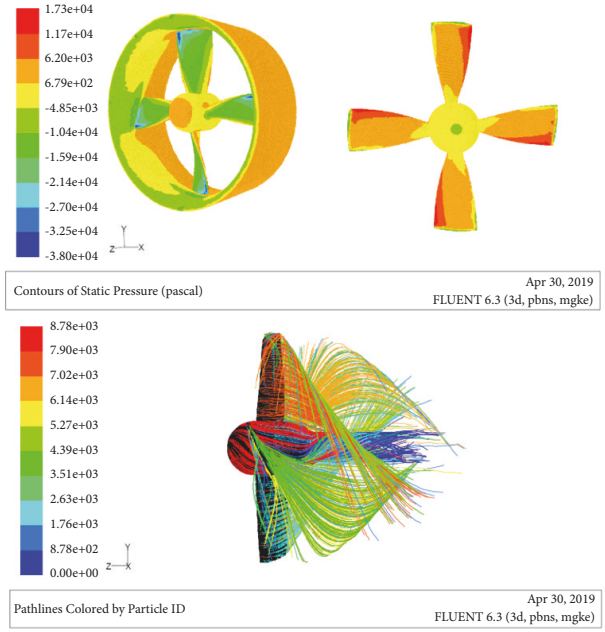

Figure 7: CFD result of tail propeller.

coupling method is SIMPLEC method, which is discretized through second-order upwind method.

3.1. Tail Thruster. According to the characteristics of ZFAUV, the speed forward is about 0-5 kn. The physical model used in CFD is shown in Figure 6.

Figure 7 shows the pressure distribution on the propeller blade surface and wake flow trace distribution at rated speed.

The thrust and torque at different flow velocity was calculated and analyzed, as shown in Table 1.

At rated speed, the thrust coefficient and torque coefficient can be obtained by the following equations:

$$T = K_T \rho D^4 * n^2 \tag{4}$$

$$Q = K_Q \rho D^5 * n^2 \tag{5}$$

The advance coefficient J and the efficiency of the propeller can be calculated by the following equations:

$$J = \frac{V_p}{nD} \tag{6}$$

$$\eta = \frac{TV_p}{2\pi nQ} = \frac{K_T}{K_Q} \cdot \frac{J}{2\pi} \tag{7}$$

So the open water performance of tail thruster at rated speed can be obtained, as shown in Figure 8.

3.2. Tunnel Thruster. Tunnel thruster is mainly used to change the heading and pitch angle of ZFAUV. The performance of tunnel thruster is deeply influenced when the forward velocity changes, accordingly influencing the turning radius and maneuverability. Therefore, it is necessary to analyze the thrust at different forward velocity.

Due to the existence of tunnel, and the fact that there's no duct, the physical model of tunnel thruster in CFD is different from that of tail thruster. Tunnel needs to be added to the

Table 2: Calculated thrust and torque of tunnel thruster at different forward velocity.

T/N Q/N•m	n/%					
	10	20	40	60	80	100
v_{flow}/m/s						
0.26	0.23	0.51	1.81	4.19	8.06	13.04
	0.003	0.007	0.026	0.058	0.110	0.176
0.56	0.25	0.81	2.22	4.43	7.74	11.87
	0.003	0.010	0.030	0.061	0.106	0.163
1.14	0.23	1.06	3.55	6.49	8.02	13.27
	0.003	0.013	0.042	0.082	0.110	0.178
1.79	0.51	1.14	3.34	7.11	15.07	17.51
	0.007	0.014	0.040	0.086	0.179	0.221
2.22	0.075	0.82	3.63	6.85	14.21	23.6
	0.002	0.011	0.042	0.083	0.167	0.279
2.87	0.075	0.74	5.30	7.64	13.41	21.41
	0.001	0.010	0.066	0.088	0.159	0.254

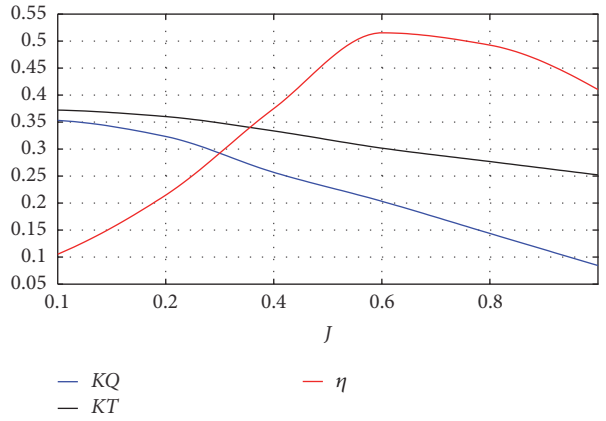

Figure 8: Open water performance at rated speed.

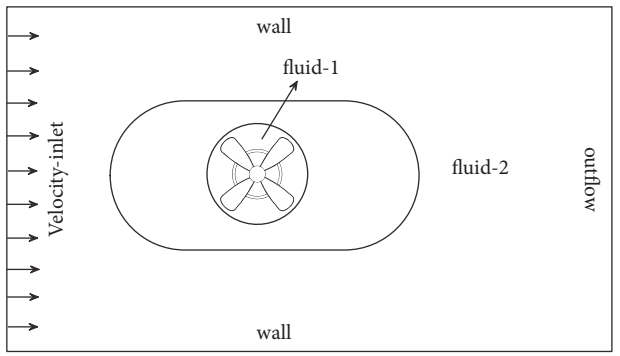

Figure 9: Physical model of tunnel thruster in CFD.

physical model, as shown in Figure 9; dynamic fluid-1 is the area where the tunnel is located.

The direction of flow is perpendicular to the axis of tunnel, so the angle between the direction of inflow and the axis of tunnel is set as 90 degrees. The physical model used in CFD is shown in Figure 9.

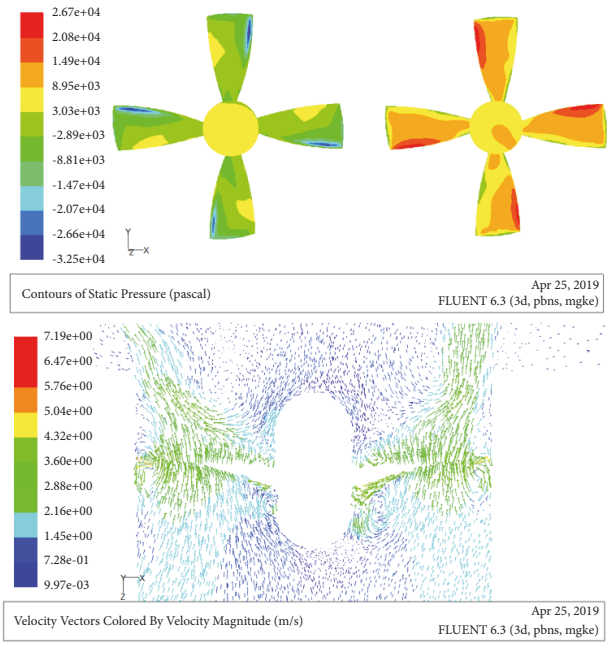

Figure 10: CFD result of tunnel thruster.

Figure 10 shows the pressure distribution on the propeller blade surface and velocity vector distribution at rated speed.

The hydrodynamic performance of tunnel thruster is calculated and analyzed for different forward velocity, the thrust and torque is shown in Table 2.

The thrust variation of tunnel thruster at different forward velocity can be drawn, as shown in Figure 11.

In order to make the simulation result more real and reliable, the thrust and torque coefficients of the tunnel thruster should be corrected in real time according to the calculated speed.

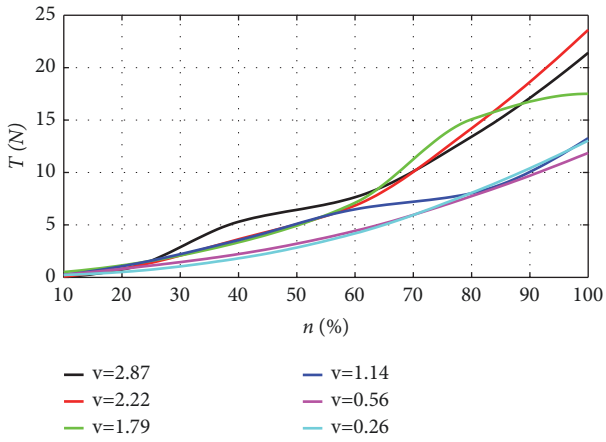

Figure 11: The thrust of tunnel thruster.

4. Motion Simulation and Maneuverability Analysis

On the basis of 6-DOF mathematical model in Section 2, we perform motion simulation and maneuverability analysis of ZFAUV. The motion simulations can be divided into two main aspects: lateral motions and longitudinal motions.

4.1. Lateral Motions. In order to study the dynamical behavior of ZFAUV in horizontal plane, including steady maneuver and zigzag maneuver, the mathematical model has to be simplified in *Bxz*.

When ZFAUV moves in horizontal plane, v, r, and Y_e are all zero, θ is very small; it can be considered that $\sin\theta = 0$, $\cos\theta = 1$. Therefore, the simplified model in horizontal plane can be obtained as follows:

$$\begin{aligned}
&(m+\lambda_{11})\,\dot{u} \\
&\quad = (T_1+T_2+T_3+T_4)\cos\vartheta + \frac{1}{2}\rho V^2{}_T S C_x(0) \\
&(m+\lambda_{33})\,\dot{w} + \lambda_{35}\dot{q} \\
&\quad = muq + \Delta G\sin\varphi \\
&\qquad + \frac{1}{2}\rho V^2{}_T S\left(C_Z^{\beta}\beta + C_Z^{p}p' + C_Z^{q}q'\right) + T_5 \\
&\qquad - (T_3 - T_4)\sin\vartheta \\
&(J_x+\lambda_{44})\,\dot{p} \\
&\quad = muy_G q + Gy_G\sin\varphi \\
&\qquad + \frac{1}{2}\rho V^2{}_T SL\left(C_R^{\beta}\beta + C_R^{p}p' + C_R^{q}q'\right) \\
&\qquad + (-Q_1 + Q_2 - Q_3 + Q_4)\cos\vartheta \\
&\left(J_y+\lambda_{55}\right)\dot{q} + \lambda_{35}\dot{w} \\
&\quad = \frac{1}{2}\rho V^2{}_T SL\left(C_M^{\beta}\beta + C_M^{p}p' + C_M^{q}q'\right) \\
&\qquad - (T_3 - T_4)\sin\vartheta L_1 - T_5 L_3 + (-Q_1 + Q_2)\sin\vartheta \\
&\qquad + Q_6 \\
&\dot{\varphi} = p \\
&\dot{\psi} = q\cos\varphi \\
&V_T = \sqrt{u^2 + w^2} \\
&\beta = \arcsin\left(\frac{w}{V_T}\right) \\
&u = V_T\cos\beta \\
&\dot{X}_e = u\cos\psi + w\sin\psi\cos\varphi \\
&\dot{Z}_e = -u\sin\psi + w\cos\psi\cos\varphi \\
&-(T_1 - T_2)\sin\vartheta L_1 + T_6 L_2 + (Q_3 - Q_4)\sin\vartheta + Q_5 = 0
\end{aligned} \tag{8}$$

4.1.1. Steady Motion in Horizontal Plane. In steady maneuver, the motion parameters remain unchanged and the acceleration parameters are zero:

$$\begin{aligned}
&\dot{\omega} = \dot{q} = \dot{p} = 0 \\
&u = V_T, \\
&p = 0, \\
&\varphi = \varphi_c \\
&q = q_c, \\
&\beta = \beta_c, \\
&n_5 = \text{const}
\end{aligned} \tag{9}$$

where subscript c means steady value. Introduce (9) into (8):

$$\boldsymbol{A}\begin{bmatrix} q_c' \\ \beta_c \\ \sin\varphi_c \end{bmatrix} = \boldsymbol{B}T_5 + \boldsymbol{C} \tag{10}$$

where

$$\boldsymbol{A} = \begin{bmatrix} a_{11} & a_{12} & a_{13} \\ a_{21} & a_{22} & a_{23} \\ a_{31} & a_{32} & a_{33} \end{bmatrix},$$

$$\boldsymbol{B} = \begin{bmatrix} b_{11} \\ b_{21} \\ b_{31} \end{bmatrix},$$

$$\boldsymbol{C} = \begin{bmatrix} c_{11} \\ c_{21} \\ c_{31} \end{bmatrix},$$

$$
\begin{aligned}
a_{11} &= \frac{mV^2{}_T}{L} + \frac{1}{2}\rho V^2{}_T S C_Z^q,\\
a_{12} &= \frac{1}{2}\rho V^2{}_T S C_Z^\beta,\\
a_{13} &= \Delta G,\\
a_{21} &= \frac{mV^2{}_T}{L} y_G + \frac{1}{2}\rho V^2{}_T S L C_R^q,\\
a_{22} &= \frac{1}{2}\rho V^2{}_T S L C_R^\beta,\\
a_{23} &= G y_G,\\
a_{31} &= \frac{1}{2}\rho V^2{}_T S L C_M^q,\\
a_{32} &= \frac{1}{2}\rho V^2{}_T S L C_M^\beta,\\
a_{33} &= 0,\\
b_{11} &= -1,\\
b_{21} &= 0,\\
b_{31} &= L_3,\\
c_{11} &= -\left(T_4 - T_3\right)\sin\vartheta,\\
c_{21} &= \left(Q_1 - Q_2 + Q_3 - Q_4\right)\cos\vartheta,\\
c_{31} &= \left(T_3 - T_4\right)\sin\vartheta L_1 + \left(Q_1 - Q_2\right)\sin\vartheta - Q_6,\\
V^2{}_T &= -\frac{2\left(T_1 + T_2 + T_3 + T_4\right)}{SC_x(0)},\\
q_c' &= \frac{q_c L}{V_T}.
\end{aligned}
\tag{11}
$$

In steady linear maneuver, $q_c' = \beta_c = \varphi_c = 0$, $T_5 = 0$, introduce this into (10):

$$
c_{11} = c_{21} = c_{31} = 0 \tag{12}
$$

$$
\begin{aligned}
&c_{11} = 0 \Longrightarrow\\
&T_3 = T_4\\
&c_{21} = 0 \Longrightarrow\\
&Q_1 = Q_2 \Longrightarrow\\
&T_1 = T_2\\
&c_{31} = 0 \Longrightarrow\\
&Q_6 = 0
\end{aligned}
\tag{13}
$$

So, ZFAUV is only possible to keep steady linear maneuver under the condition of $T_1 = T_2$, $T_3 = T_4$, and $T_5 = T_6 = 0$. In order to achieve steady linear maneuver, propeller-rudder AUVs have to use differential rudder, but the effective range of rudder will be reduced; it also increases the complexity of structure design and program design. With the four fixed thrusters of ZFAUV, this problem can be solved simply and effectively.

When ZFAUV is moving forward, if the tunnel thruster is executed, lateral force and yaw moment will be produced. Under the action of lateral force and yaw moment, ZFAUV will turn left or turn right.

According to (10), the following can be obtained:

$$
\begin{bmatrix} q_c' \\ \beta_c \\ \sin\varphi_c \end{bmatrix} = \boldsymbol{A}^{-1}\boldsymbol{B}T_5 + \boldsymbol{A}^{-1}\boldsymbol{C} = \boldsymbol{D}T_5 + \boldsymbol{E} \tag{14}
$$

where

$$
\boldsymbol{D} = \frac{1}{|\boldsymbol{A}|}\begin{bmatrix} d_{11} \\ d_{21} \\ d_{31} \end{bmatrix},
$$

$$
\boldsymbol{E} = \frac{1}{|\boldsymbol{A}|}\begin{bmatrix} e_{11} \\ e_{21} \\ e_{31} \end{bmatrix},
$$

$$
\begin{aligned}
|\boldsymbol{A}| &= \mathrm{a}_{11}\mathrm{a}_{22}\mathrm{a}_{33} - \mathrm{a}_{11}\mathrm{a}_{23}\mathrm{a}_{32} - \mathrm{a}_{21}\mathrm{a}_{12}\mathrm{a}_{33} + \mathrm{a}_{21}\mathrm{a}_{13}\mathrm{a}_{32}\\
&\quad + \mathrm{a}_{31}\mathrm{a}_{12}\mathrm{a}_{23} - \mathrm{a}_{31}\mathrm{a}_{13}\mathrm{a}_{22},\\
d_{11} &= \left(\mathrm{a}_{22}\mathrm{a}_{33} - \mathrm{a}_{23}\mathrm{a}_{32}\right)\mathrm{b}_{11} - \left(\mathrm{a}_{12}\mathrm{a}_{33} - \mathrm{a}_{13}\mathrm{a}_{32}\right)\mathrm{b}_{21}\\
&\quad + \left(\mathrm{a}_{12}\mathrm{a}_{23} - \mathrm{a}_{13}\mathrm{a}_{22}\right)\mathrm{b}_{31},\\
d_{21} &= -\left(\mathrm{a}_{21}\mathrm{a}_{33} - \mathrm{a}_{23}\mathrm{a}_{31}\right)\mathrm{b}_{11} + \left(\mathrm{a}_{11}\mathrm{a}_{33} - \mathrm{a}_{13}\mathrm{a}_{31}\right)\mathrm{b}_{21}\\
&\quad - \left(\mathrm{a}_{11}\mathrm{a}_{23} - \mathrm{a}_{13}\mathrm{a}_{21}\right)\mathrm{b}_{31},\\
d_{31} &= \left(\mathrm{a}_{21}\mathrm{a}_{32} - \mathrm{a}_{22}\mathrm{a}_{31}\right)\mathrm{b}_{11} - \left(\mathrm{a}_{11}\mathrm{a}_{32} - \mathrm{a}_{12}\mathrm{a}_{31}\right)\mathrm{b}_{21}\\
&\quad + \left(\mathrm{a}_{11}\mathrm{a}_{22} - \mathrm{a}_{12}\mathrm{a}_{21}\right)\mathrm{b}_{31},\\
e_{11} &= \left(\mathrm{a}_{22}\mathrm{a}_{33} - \mathrm{a}_{23}\mathrm{a}_{32}\right)\mathrm{c}_{11} - \left(\mathrm{a}_{12}\mathrm{a}_{33} - \mathrm{a}_{13}\mathrm{a}_{32}\right)\mathrm{c}_{21}\\
&\quad + \left(\mathrm{a}_{12}\mathrm{a}_{23} - \mathrm{a}_{13}\mathrm{a}_{22}\right)\mathrm{c}_{31},\\
e_{21} &= -\left(\mathrm{a}_{21}\mathrm{a}_{33} - \mathrm{a}_{23}\mathrm{a}_{31}\right)\mathrm{c}_{11} + \left(\mathrm{a}_{11}\mathrm{a}_{33} - \mathrm{a}_{13}\mathrm{a}_{31}\right)\mathrm{c}_{21}\\
&\quad - \left(\mathrm{a}_{11}\mathrm{a}_{23} - \mathrm{a}_{13}\mathrm{a}_{21}\right)\mathrm{c}_{31},\\
e_{31} &= \left(\mathrm{a}_{21}\mathrm{a}_{32} - \mathrm{a}_{22}\mathrm{a}_{31}\right)\mathrm{c}_{11} - \left(\mathrm{a}_{11}\mathrm{a}_{32} - \mathrm{a}_{12}\mathrm{a}_{31}\right)\mathrm{c}_{21}\\
&\quad + \left(\mathrm{a}_{11}\mathrm{a}_{22} - \mathrm{a}_{12}\mathrm{a}_{21}\right)\mathrm{c}_{31}.
\end{aligned}
\tag{15}
$$

Therefore,

$$
\begin{aligned}
q_c' &= \frac{1}{|\boldsymbol{A}|}d_{11}T_5 + \frac{1}{|\boldsymbol{A}|}e_{11}\\
\beta_c &= \frac{1}{|\boldsymbol{A}|}d_{21}T_5 + \frac{1}{|\boldsymbol{A}|}e_{21}\\
\varphi_c &= \arcsin\left(\frac{1}{|\boldsymbol{A}|}d_{31}T_5 + \frac{1}{|\boldsymbol{A}|}e_{31}\right)
\end{aligned}
\tag{16}
$$

Table 3: Turning radius of ZFAUV at different speed.

Forward	Tunnel				
	20%	40%	60%	80%	100%
20%(0.56m/s)	6.1	3.3	2.8	2.5	2
40%(1.14m/s)	13.2	9.5	8	5.8	4.4
60%(1.79m/s)	29	20	14	10.5	8.2
80%(2.22m/s)	52	30	20	15	12
100%(2.87m/s)	72	38.5	26	21	17

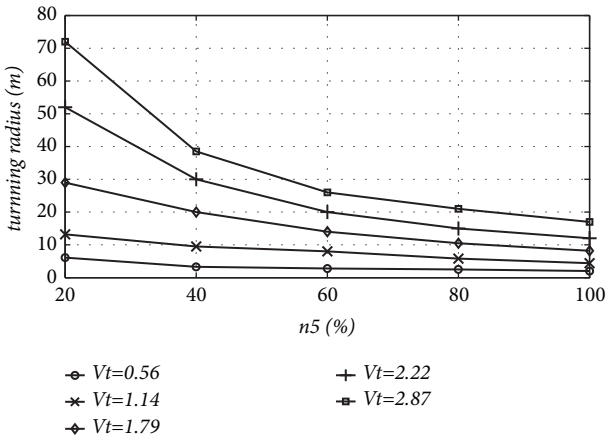

Figure 12: Turning radius at different speed.

The turning radius is as follows:

$$R_c = \frac{V_T}{|q_c|} = \frac{L}{|q_c'|} \tag{17}$$

The relationship between the turning radius and the speed of tunnel thruster is shown in Table 3.

As can be seen from Table 4 and Figure 12, at a certain tunnel thruster speed, the greater the speed forward, the larger the turning radius. Different from propeller-rudder AUVs, the turning radius is the same at a given rudder angle [26].

4.1.2. Zigzag Maneuver. Zigzag maneuver is widely used to evaluate the maneuverability of ships and torpedoes, so this can be used to evaluate the maneuverability of ZFAUV.

In a general zigzag maneuver, the vehicle is moving forward at constant speed and the rudder is executed to a specified maximum rudder angle in one direction at maximum rudder rate. The vehicle responds by turning in that direction. When the vehicle heading angle reaches a specified check heading angle, the rudder is turned at maximum rudder rate in the opposite direction until it reaches the maximum rudder angle specified. The vehicle reacts by turning in the opposite direction, and the procedure is repeated when the check heading angle in the opposite direction is reached. This results in a zigzag response that is used to assess the maneuverability of the vehicle. The maximum rudder angle and the check heading angle characterize the maneuver type; for instance, a

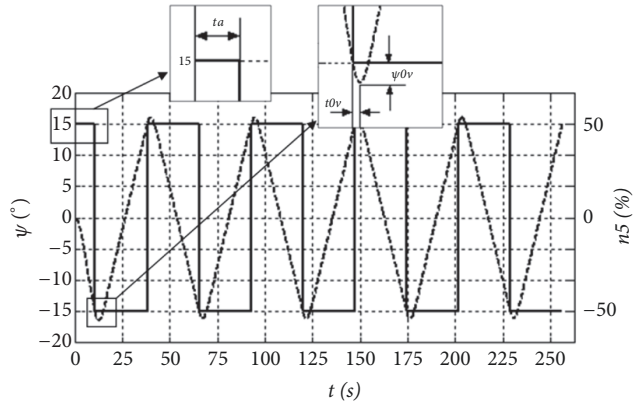

Figure 13: Performance of heading zigzag maneuver.

20/10 zigzag maneuver turns the rudders to 20° and changes direction when the check heading angle of 10° is reached [27–29].

For ZFAUV, the direction is controlled by tunnel thruster or differential control of tail thrusters; behind, tunnel thruster or differential control of tail thrusters is replaced by 'rudder'. So the 50%/15° zigzag maneuver is adopted in this study;, that is, when ZFAUV is moving forward at constant speed, the 'rudder' is executed to 50% (the first execute), ZFAUV starts to turn right. Once the check heading angle of -15° is reached for the first execute, the 'rudder' is executed to -50% (the second execute). At this time, ZFAUV will continue to turn right because of inertia, but the turning rate gradually decreases. When $q = 0$, ZFAUV starts to turn left. Once the check heading angle of 15° is detected for the second execute, the 'rudder' is executed to 50% (the third execute). So it is repeated 5 times. Figure 13 shows the performance of ZFAUV in zigzag maneuver simulation.

The characteristic parameters of zigzag maneuver include the initial turning period, the overshoot time, the overshoot heading angle, and the full cycle. The smaller the characteristic parameters, the better the heading changing ability of ZFAUV.

The initial turning period (t_a), as shown in Figure 13, is the time between the first 'rudder' execute and the second 'rudder' execute. It indicates the ability to change heading. Usually, the dimensionless form of the initial turning period is used as the criterion of the heading changing ability; that is, $t_a' = t_a(V_T/L)$.

The overshoot time (t_{0v}) is the time from the second 'rudder' execute to ZFAUV stop turning in the original direction ($q = 0$).

After the second execute, ZFAUV keeps turning in the original direction. The overshoot heading angle (ψ_{0v}) is the difference between the maximum yaw angle and the steering yaw angle (15°).

The characteristic parameters of ZFAUV at different speed can be obtained, as shown in Tables 4 and 5, Figures 14 and 15. It can be seen from the figures that with the increase of the speed, the ability to change heading becomes worse gradually.

Table 4: Heading zigzag parameters-tunnel control (50%).

Forward speed (%)	10	20	40	60	80	100
V_T *(m/s)*	0.26	0.56	1.14	1.79	2.22	2.87
t_a *(s)*	8.50	6.31	6.38	8.19	9.69	12.00
t_a'	2.21	1.77	3.64	7.33	10.76	17.22
$t_{0v}(s)$	6.50	3.25	1.63	1.03	0.83	0.63
$\psi_{0v}(^\circ)$	38.6	11.8	2.9	1.2	0.8	0.5

Table 5: Heading zigzag parameters-differential control (50%).

Forward speed (%)	10	20	40	60	80	100
V_T *(m/s)*	0.16	0.39	0.81	1.27	1.57	2.03
t_a *(s)*	6.25	5.31	4.13	4.00	4.25	4.94
t_a'	1.00	1.04	1.67	2.54	3.34	5.01
$t_{0v}(s)$	5.85	3.88	1.98	1.23	0.98	0.75
$\psi_{0v}(^\circ)$	60.6	31.1	9.5	4.2	2.4	1.7

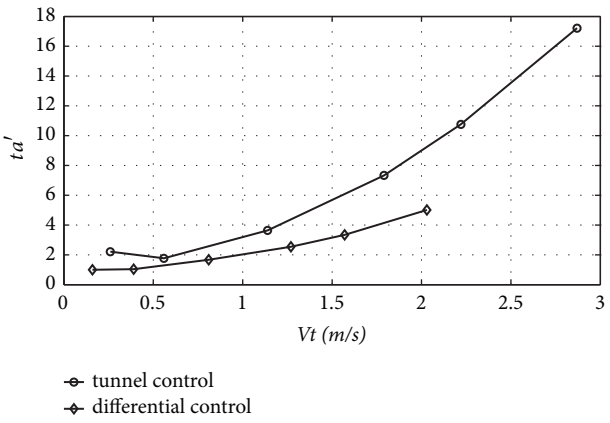

Figure 14: t_a' at different speed in horizontal plane.

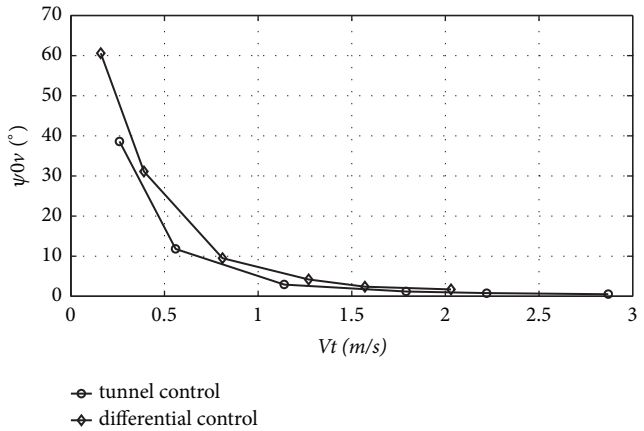

Figure 15: ψ_{0v} at different speed in horizontal plane.

From Figures 14 and 15, we can get the following conclusions:

(1) Same as propeller-rudder AUVs [23], the heading changing ability of ZFAUV becomes worse with the increase of speed, and the overshoot yaw angle decreases with the increase of speed. Tunnel control has poor heading changing ability, but its overshoot yaw angle is smaller; differential control has better heading changing ability, but the overshoot yaw angle is larger. Comparatively, the maneuverability of differential control is better than that of tunnel control, but differential control is at the cost of losing speed. When the demand for speed is higher, the heading accuracy should be reduced, so tunnel control can be used, and differential control can be used when high heading precision is needed.

(2) Compared with ordinary propeller-rudder AUVs, the overshoot angle of ZFAUV is larger at low speed. The reason is that the steering force and moment of ZFAUV, whether controlled by differential or tunnel, is independent of the forward speed. At low speed, steering force and moment is more powerful than forward force; this results in larger overshoot. But the rudder efficiency of ordinary propeller-rudder AUVs is related to speed. So, ZFAUV is more advantageous at low speed when good maneuverability is required.

4.1.3. Turning around In Situ. As shown in Figures 3(h) and 3(i), ZFAUV can turn around the center of buoyancy in situ when certain conditions are satisfied; that is, the turning radius is zero. When stable state is achieved, the motion parameters remain unchanged and the acceleration parameters are zero:

$$\begin{aligned} u &= 0, \\ w &= 0, \\ V_T &= 0 \\ \dot{u} &= 0, \\ \dot{w} &= 0 \\ \varphi &= \varphi_c, \\ \dot{\varphi} &= 0 \end{aligned} \tag{18}$$

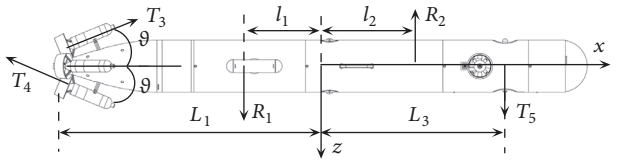

Figure 16: Force analysis when turning around in situ.

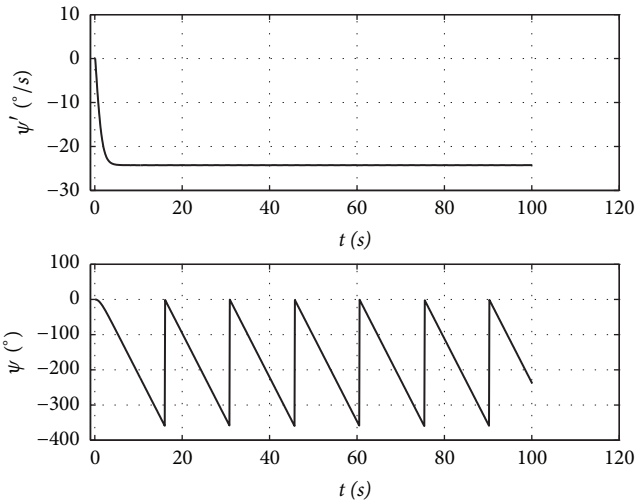

Figure 17: Simulation result of turning around in situ.

Table 6: Angular velocity of turning around in situ.

$n5(\%)$	10	20	40	60	80	100
$\psi'(^\circ/s)$	0.2	0.9	3.8	8.6	15.3	24.1

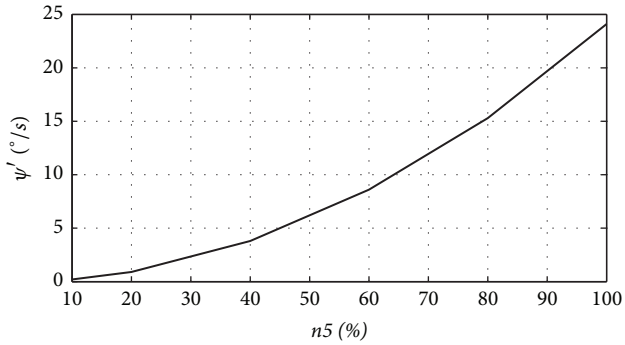

Figure 18: Angular velocity of turning around in situ.

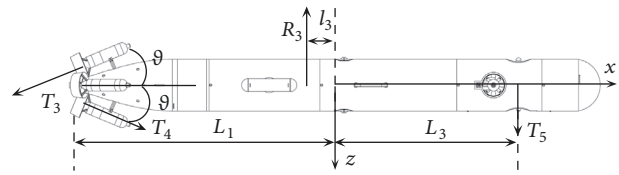

Figure 19: Force analysis when moving lateral.

Then, the force acting on ZFAUV is shown in Figure 16, including thrust (T_3,T_4,T_5) and equivalent fluid viscous resistance (R_1,R_2). The equivalent location of R_1 and R_2 can be obtained by CFD simulation:

$$\begin{aligned} 2T_3 \sin\vartheta + R_2 &= T_5 + R_1 \\ 2T_3 \sin\vartheta L_1 + T_5 L_3 &= R_1 l_1 + R_2 l_2 \end{aligned} \tag{19}$$

after stable state is achieved.

The equation of rotating along y-axis can be simplified as follows:

$$\begin{aligned} \left(J_y + \lambda_{55}\right)\dot{q} &= -\left(T_3 - T_4\right)\sin\vartheta L_1 - T_5 L_3 + R_1 l_1 \\ &\quad + R_2 l_2 \\ \dot{\psi} &= q\cos\varphi \end{aligned} \tag{20}$$

where

$$\begin{aligned} T_3 &= -T_4 \\ R_1 &= \frac{1}{2}\rho q^2 L^2 C_{q1} S_q \\ R_2 &= \frac{1}{2}\rho q^2 L^2 C_{q2} S_q \end{aligned} \tag{21}$$

Figure 17 is the simulation result of $n_5 = 100\%$.

The relationship between turning angular velocity and n_5 is shown in Table 6 and Figure 18.

From Figure 18 and Table 6, it can be concluded that, after stable state is achieved, the turning angular velocity increases with the increase of n_5, and the maximum turning angular velocity is about 24.1°/s.

4.1.4. Moving Lateral. As shown in Figures 3(f) and 3(g), ZFAUV can move lateral when certain conditions are satisfied. When stable state is achieved, the motion parameters remain unchanged and the acceleration parameters are zero. Then, the force acting on ZFAUV is shown in Figure 19, including thrust (T_3,T_4,T_5) and equivalent fluid viscous resistance (R_3). For the asymmetry of the geometrical shape, the location of R_3 is a distance away from the buoyancy (l_3). l_3 can be obtained by CFD simulation.

$-2T_3 \sin\vartheta(L_1 - l_3) = T_5(L_3 + l_3)$ after stable state is achieved.

The equation along z-axis can be simplified as follows:

$$\begin{aligned} \dot{Z}_e &= w \\ \left(m + \lambda_{33}\right)\dot{w} &= T_5 - \left(T_3 - T_4\right)\sin\vartheta - R_1 \end{aligned} \tag{22}$$

where

$$\begin{aligned} T_3 &= -T_4 \\ R_3 &= \frac{1}{2}\rho\omega^2 C_Z S_Z \end{aligned} \tag{23}$$

Figure 20 is the simulation result of $n_5 = 100\%$.

The maximum velocity of moving lateral is about 0.39m/s.

4.2. Longitudinal Motions. In order to study the dynamical behavior of ZFAUV in vertical plane, including steady

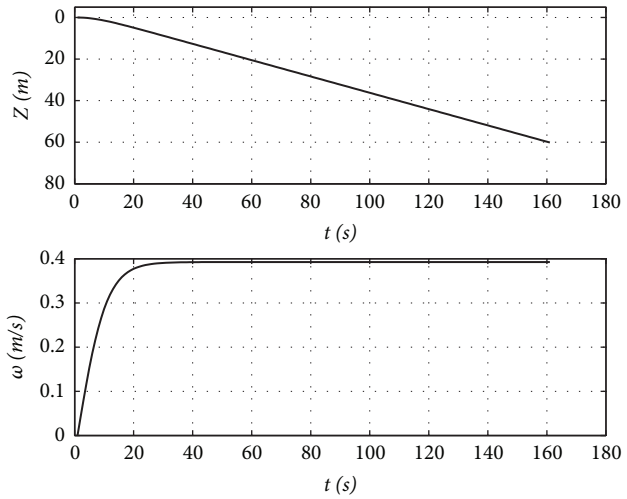

Figure 20: Simulation result of moving lateral.

maneuver and trapezoidal steering maneuver, the mathematical model has to be simplified in Bxy.

When ZFAUV moves in vertical plane, $\beta, w, p, q, \varphi, \psi, Z_e$ are all zero. Therefore, the simplified model in vertical plane can be obtained as follows:

$$\begin{aligned}
&(m+\lambda_{11})\dot{u} \\
&\quad = mvr - \Delta G\sin\theta + (T_1+T_2+T_3+T_4)\cos\vartheta \\
&\qquad + \frac{1}{2}\rho V^2{}_T S C_x(0) \\
&(m+\lambda_{22})\dot{v} + \lambda_{26}\dot{r} \\
&\quad = -mur - \Delta G\cos\theta + (T_1-T_2)\sin\vartheta + T_6 \\
&\qquad + \frac{1}{2}\rho V^2{}_T S\left(C_Y^{\alpha}\alpha + C_Y^{r}r'\right) \\
&(J_z+\lambda_{66})\dot{r} + \lambda_{26}\dot{v} \\
&\quad = Gy_G\sin\theta + \frac{1}{2}\rho V^2{}_T SL\left(C_N^{\alpha}\alpha + C_N^{r}r'\right) \\
&\qquad - (T_1-T_2)\sin\vartheta L_1 + T_6L_2 + (Q_3-Q_4)\sin\vartheta \\
&\qquad + Q_5 \\
&\dot{\theta} = r \\
&\dot{X}_e = u\cos\theta - v\sin\theta \\
&\dot{Y}_e = u\sin\theta + v\cos\theta \\
&V_T = \sqrt{u^2+v^2} \\
&\alpha = \arctan\left(-\frac{v}{u}\right) \\
&-(T_3-T_4)\sin\vartheta L_1 - T_5L_3 + (-Q_1+Q_2)\sin\vartheta + Q_6 \\
&\quad = 0
\end{aligned} \tag{24}$$

4.2.1. Steady Maneuver in Vertical Plane. In steady maneuver of ZFAUV, the motion parameters remain unchanged and the acceleration parameters are zero:

$$\begin{aligned}
&\dot{u} = \dot{v} = \dot{r} = 0 \\
&u = u_c, \\
&v = v_c, \\
&\theta = \theta_c \\
&r = 0, \\
&n_6 = \text{const}
\end{aligned} \tag{25}$$

where subscript c means steady value. Introduce (25) into (24):

$$\begin{aligned}
&-\Delta G\sin\theta + (T_1+T_2+T_3+T_4)\cos\vartheta \\
&\quad + \frac{1}{2}\rho V^2{}_T SC_x(0) = 0 \\
&-\Delta G\cos\theta + (T_1-T_2)\sin\vartheta + T_6 + \frac{1}{2}\rho V^2{}_T SC_Y^{\alpha}\alpha = 0 \\
&Gy_G\sin\theta + \frac{1}{2}\rho V^2{}_T SLC_N^{\alpha}\alpha - (T_1-T_2)\sin\vartheta L_1 \\
&\quad + T_6L_2 + (Q_3-Q_4)\sin\vartheta + Q_5 = 0
\end{aligned} \tag{26}$$

After simplification, the following can be obtained:

$$a\sin^2\theta_c + b\sin\theta_c + c = 0 \tag{27}$$

where $a = d^2 + e^2$, $b = -2df$, $c = f^2 - e^2$, $d = Gy_GC_Y^{\alpha}$, $e = \Delta GC_N^{\alpha}L$, $f = gC_Y^{\alpha} + hLC_N^{\alpha}$, $g = (T_1-T_2)\sin\vartheta L_1 - T_6L_2 - (Q_3-Q_4)\sin\vartheta - Q_5$, and $h = (T_1-T_2)\sin\vartheta + T_6$.

In order to ensure the safety of ZFAUV, the range of pitch angle is limited as $\theta \in [-30^{\circ}, 30^{\circ}]$; therefore, $\sin\theta \in [-1/2, 1/2]$. $d \neq 0, e \neq 0 \Longrightarrow a \neq 0$; the following can be obtained:

$$\begin{aligned}
&b^2 - 4ac \geq 0 \\
&-\frac{1}{2} \leq \frac{-b \pm \sqrt{b^2-4ac}}{2a} \leq \frac{1}{2}
\end{aligned} \tag{28}$$

According to (28), the reasonable range of T_6, or T_1 and T_2 can be obtained.

If $T_1 = T_2$, $T_3 = T_4$, θ is determined by T_6. This is the main difference between ZFAUV and ordinary propeller-rudder AUVs. ZFAUV can still change the pitch angle without forward speed. Propeller-rudder AUVs can change its attitude only if the forward speed exists.

4.2.2. Trapezoidal Steering. Trapezoidal steering maneuver is the most typical test to verify the maneuverability in vertical plane; it is of great significance to the study of deep maneuvering motion [30, 31].

In a general trapezoidal steering maneuver, the vehicle is moving forward at constant speed and the 'rudder' is

Table 7: Trapezoidal steering parameters-tunnel control (30%).

Forward speed (%)	10	20	40	60	80	100
V_T *(m/s)*	0.33	0.56	1.14	1.79	2.22	2.87
t_e *(s)*	3.62	3.62	4.12	4.87	5.62	6.75
$\theta_{0v}(^\circ)$	12.8	7.8	3.4	1.6	1.2	0.8
$\xi_{0v}(m)$	0.21	0.98	2.29	4.20	5.96	9.13

Table 8: Trapezoidal steering parameters-differential control (30%).

Forward speed (%)	10	20	40	60	80	100
V_T *(m/s)*	0.25	0.39	0.81	1.27	1.57	2.03
t_e *(s)*	3.75	3.75	4.12	5.00	5.87	7.5
$\theta_{0v}(^\circ)$	3.0	2.5	1.1	0.4	0.2	0.1
ξ_{0v} *(m)*	-0.22	0.03	0.24	0.45	0.63	0.96

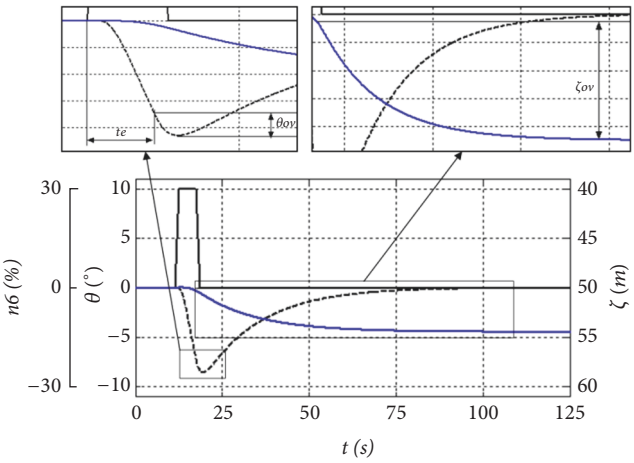

Figure 21: Simulation result of trapezoidal steering.

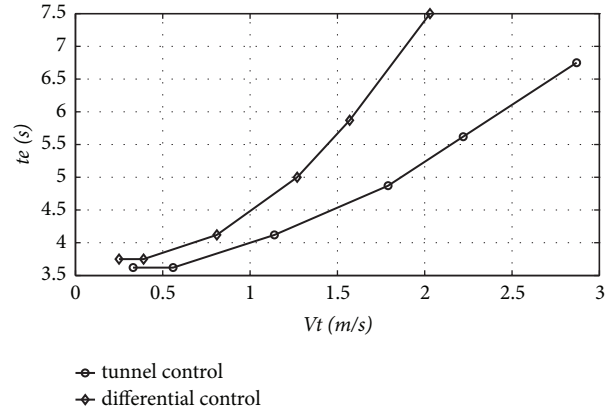

Figure 22: t_e of trapezoidal steering.

executed to a specified 'rudder' angle (δ_0) at certain 'rudder' rate. The pitch angle will change accordingly. When the specified check pitch angle (θ_e) is reached, the 'rudder' is set as zero, the depth will continue to increase, and the pitch angle will continue to increase also and gradually return to zero due to its righting moment effect. Then, the vehicle will move forward at another depth. The whole process is a complete vertical trapezoidal steering maneuver; for ZFAUV, it can be expressed as

$$n_6(t) = \begin{cases} \dot{n}_6 \cdot t & t \le t_1 \\ n_0 & t_1 \le t \le t_2 \\ n_0 - \dot{n}_6 \cdot (t - t_2) & t_2 \le t \le t_3 \end{cases} \quad (29)$$

where $\dot{n}_6 = n_0/t_0$, n_0, t_0 are the command tunnel speed and the command time, respectively.

Figure 21 shows the performance of ZFAUV in trapezoidal steering maneuver.

The characteristic parameters of trapezoidal steering maneuver include the execution time, the overshoot pitch angle, and the overshoot depth. The smaller the characteristic parameters, the better the depth changing ability of ZFAUV.

The execution time (t_e), as shown in Figure 21, is the time from the 'rudder' execute to the check pitch angle (θ_e) is reached. The smaller the t_e, the better the maneuverability in vertical plane.

After the 'rudder' is executed to zero, the pitch angle will continue to increase and gradually return to zero. The overshoot pitch angle (θ_{0v}) is the difference between the maximum pitch angle and the check pitch angle (7°).

The overshoot depth (Y_{e0v}) is the difference between the extreme depth after the second 'rudder' execute and the depth at the second 'rudder' execute, as shown in Figure 21.

The maximum 'rudder' angle and the check pitch angle characterize the maneuver type; for instance, a 10/7 trapezoidal steering maneuver turns the 'rudder' to 10° and set as 0 when the check pitch angle of 7° is reached. For ZFAUV, 30%/7° trapezoidal steering maneuver is adopted. The characteristic parameters at different speed can be obtained, as shown in Tables 7 and 8, Figures 22–24.

From Figures 22–24, we can get the following conclusions:

(1) Different with ordinary propeller-rudder AUVs (t_e becomes smaller with the increase of velocity), t_e of ZFAUV becomes larger with the increase of velocity. t_e of tunnel control is smaller than that of differential control.

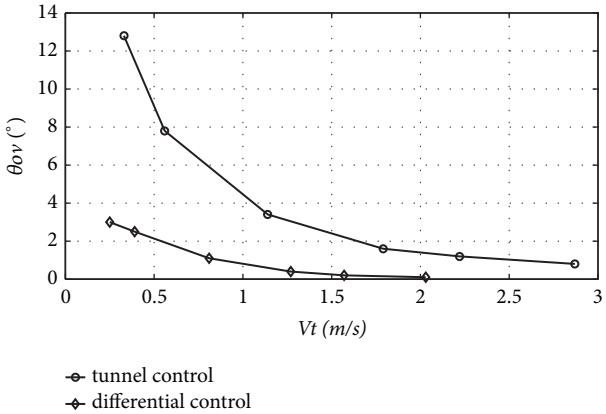

Figure 23: θ_{0v} of trapezoidal steering.

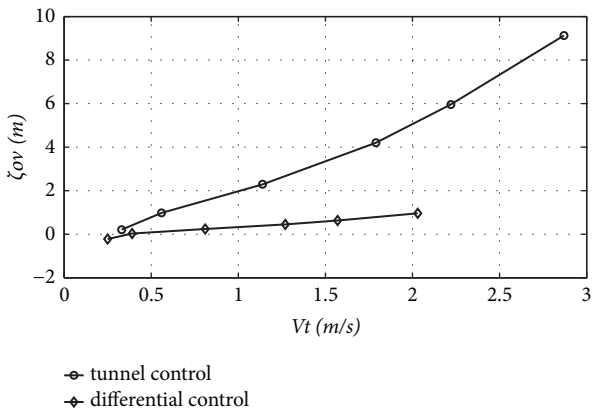

Figure 24: ξ_{0v} of trapezoidal steering.

(2) Different with ordinary propeller-rudder AUVs (θ_{0v} becomes larger with the increase of velocity), θ_{0v} of ZFAUV becomes smaller with the increase of velocity. θ_{0v} of tunnel control is larger than that of differential control.

(3) Same as ordinary propeller-rudder AUVs, ξ_{0v} becomes larger with the increase of velocity. ξ_{0v} of tunnel control is larger than that of differential control.

(4) Comparatively, the depth changing ability of differential control is better than that of tunnel control.

(5) At low speed, the depth mobility of ZFAUV is better than that of ordinary propeller rudder AUV [27, 28]; at high speed, the depth mobility of ZFAUV is worse.

4.2.3. Moving up/down Vertical. As shown in Figures 4(f) and 4(g), ZFAUV can move up/down vertical when certain conditions are satisfied. When stable state is achieved, the motion parameters remain unchanged and the acceleration parameters are zero. Then, the force acting on ZFAUV is shown in Figure 25, including thrust (T_1, T_2, T_6), net buoyancy ($\triangle G = G - B$), and equivalent fluid viscous resistance (R_4). For the asymmetry of the geometrical shape, the location of R_4 is a distance away from the buoyancy (l_4). l_4 can be obtained by CFD simulation.

$-2T_1 \sin\vartheta(L_1 - l_4) = -T_6(L_3 + l_4) + \triangle G l_4$ after stable state is achieved.

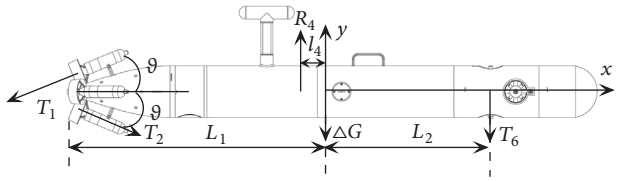

Figure 25: Force analysis when moving down vertical.

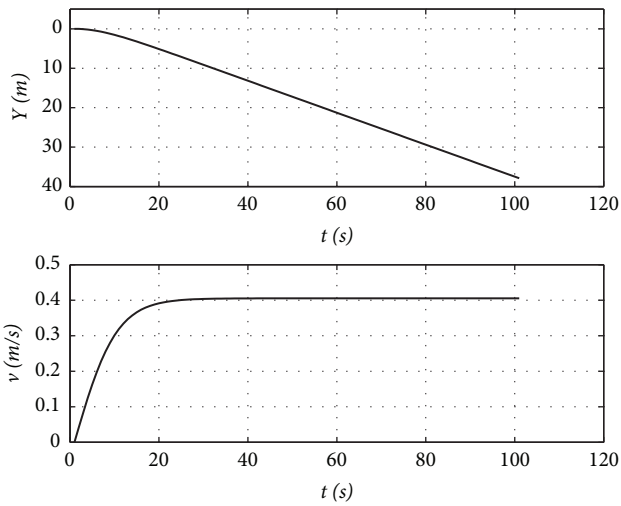

Figure 26: Simulation result of moving down vertical.

The equation along y-axis can be simplified as follows:

$$\begin{aligned} \dot{Y}_e &= v \\ (m + \lambda_{22})\,\dot{w} &= -\triangle G + (T_1 - T_2)\sin\vartheta + T_6 - R_2 \end{aligned} \tag{30}$$

where

$$\begin{aligned} T_1 &= -T_2 \\ R_2 &= \frac{1}{2}\rho v^2 C_Y S_Y \end{aligned} \tag{31}$$

Figure 26 is the simulation result of $n_6 = 100\%$.

The maximum velocity in the vertical direction is about 0.41m/s, which is slightly larger than that in the horizontal direction. For the influence of antenna, the area of ZFAUV in horizontal direction is little larger than that in vertical direction, so the steady moving velocity in horizontal direction is relatively low.

5. Application Example of Dynamics Analysis

Path tracking is the basis of motion control of AUVs, and path tracking strategy and control algorithm are needed. Line-of-Sight (LOS) guidance is the most widely used guidance strategy, and PID is the most widely used controller. For PID controller, it is necessary to adjust the parameters. If the parameters of PID are not adjusted properly, the final effect will be greatly affected.

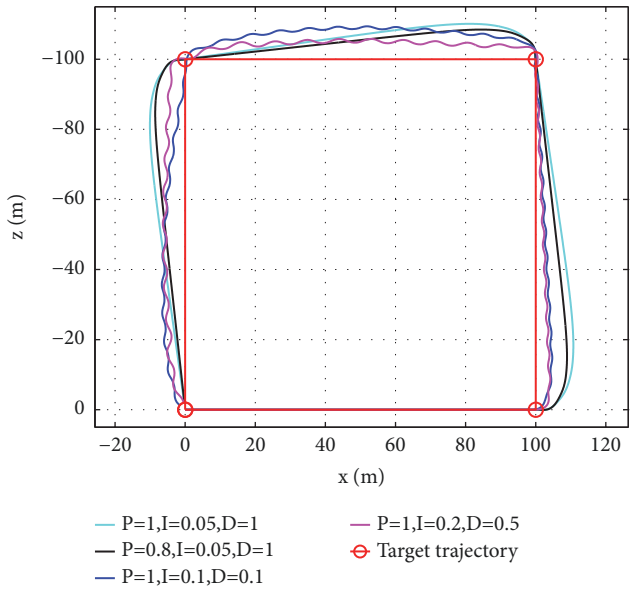

Figure 27: Tracking effect with different PID parameters.

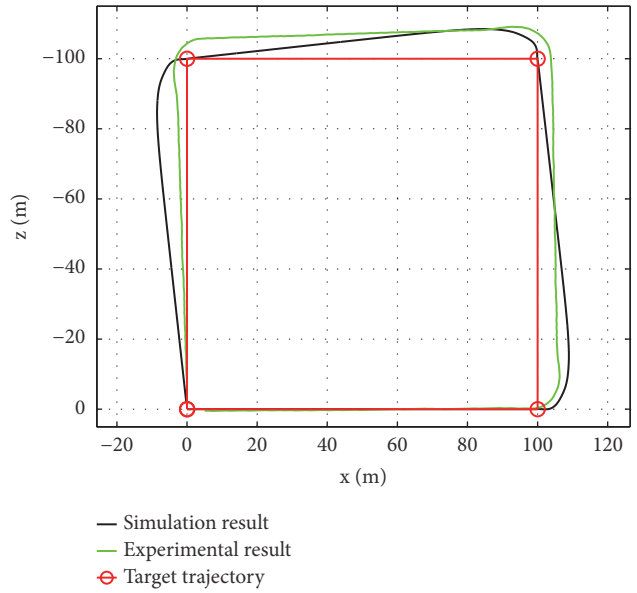

Figure 28: Experimental result of path tracking with the same parameters.

By using the mathematical model and LOS path tracking algorithm, the effect of path tracking is optimized by modifying the PID parameters. Figure 27 shows the effects of several different PID parameters, black (P=0.8, I=0.05, D=1), cyan (P=1, I=0.05, D=1), blue (P=1, I=0.1, D=0.1), and magenta (P=1, I=0.2, D=0.5). It can be seen from Figure 27 that the tracking error of black (P=0.8, I=0.05, D=1) is smaller than that of cyan (P=1, I=0.05, D=1). When blue (P=1, I=0.1, D=0.1) or magenta (P=1, I=0.2, D=0.5) is adopted, ZFAUV shakes seriously during sailing; this will seriously affect the operation of acoustic and optical sensors. So, the tracking effect is better when P=0.8, I=0.05, D=1.

The same parameters (P=0.8, I=0.05, D=1) are adopted in water experiment, as shown in Figure 28, green. Because of the difference between ZFAUV and mathematical model, the results cannot be exactly the same; the experimental result is in good agreement with the simulation result (Figure 28, black).

These PID parameters can be tuned in one hour in the simulation system. If the parameters are tuned by water experiment, it will take about 5-7 days, which will waste a lot of time and money. This further highlights the importance of dynamic analysis and simulation.

6. Conclusion

For ZFAUV, there are four fixed thrusters at tail, and two tunnel thrusters are set at front. The maneuverability of ZFAUV is relatively high. Through the establishment of mathematical model and maneuverability analysis, the following conclusions can be drawn:

(1) The maneuverability of ZFAUV is better than ordinary propeller-rudder AUVs. Some actions that ordinary propeller-rudder AUVs cannot achieve, such as turning around in situ, moving lateral, moving up/down vertical, etc., can be achieved. Particularly, in the absence of forward speed, it can also change yaw and pitch. Different from ordinary AUVs, the turning radius is related to speed forward. The smaller the speed forward, the smaller the turning radius.

(2) ZFAUV can change yaw and pitch by tunnel thrusters or differential control of tail thrusters, but differential control will reduce the forward force. According to actual needs, the driving mode can be chosen flexibly.

(3) Same as ordinary propeller-rudder AUVs, the heading maneuverability of ZFAUV becomes worse with the increase of speed. In general, the maneuverability of differential control is better than that of tunnel control.

(4) The depth maneuverability of ZFAUV becomes worse with the increase of speed, and the depth maneuverability of differential control is better than that of tunnel control.

(5) Through numerical simulation, reasonable PID parameters can be quickly tuned, and the experiment result is in good agreement with the simulation result, this can save a lot of time and money.

The research results of this paper have guiding significance for the future development of AUVs.

Data Availability

Some data used to support the findings of this study are included within the article; others are available from the corresponding author upon request.

Conflicts of Interest

The authors declare that there are no conflicts of interest regarding the publication of this article.

Acknowledgments

This research is supported by the National Natural and Science Foundation of Hebei (No. E2018202259) and Scientific Research Project of Tianjin Education Commission (No. 2017KJ022).

References

[1] M. Ataei and A. Yousefi-Koma, "Three-dimensional optimal path planning for waypoint guidance of an autonomous underwater vehicle," *Robotics and Autonomous Systems*, vol. 67, pp. 23–32, 2015.

[2] F. Azarsina and C. D. Williams, "Manoeuvring simulation of the MUN Explorer AUV based on the empirical hydrodynamics of axi-symmetric bare hulls," *Applied Ocean Research*, vol. 32, no. 4, pp. 443–453, 2010.

[3] Y. Zhang, Y. Li, Y. Sun, J. Zeng, and L. Wan, "Design and simulation of X-rudder AUV's motion control," *Ocean Engineering*, vol. 137, pp. 204–214, 2017.

[4] A. Kukulya, A. Plueddemann, T. Austin et al., "Under-ice operations with a REMUS-100 AUV in the Arctic," in *Proceedings of the 2010 IEEE/OES Autonomous Underwater Vehicles, AUV 2010*, September 2010.

[5] L. Meng, Y. Lin, R. Zheng et al., "Mechanical design and implementation of a modular autonomous underwater vehicle," *Jiqiren/Robot*, vol. 38, no. 4, pp. 395–401, 2016.

[6] M. J. Doble, A. L. Forrest, P. Wadhams, and B. E. Laval, "Through-ice AUV deployment: Operational and technical experience from two seasons of Arctic fieldwork," *Cold Regions Science and Technology*, vol. 56, no. 2-3, pp. 90–97, 2009.

[7] A. Palmer, G. E. Hearn, and P. Stevenson, "Modelling tunnel thrusters for autonomous underwater vehicles," *IFAC Proceedings Volumes*, vol. 41, no. 1, pp. 91–96, 2008.

[8] S. Willcox and B. Joseph, "Bluefin-12 based system solution for the US Navy's surface mine counter-measures unmanned underwater vehicle program: increment 2 (SMCM/UUV-2)," 2006, http://www.bluefinrobotics.com.

[9] R. B. Wynn, V. A. I. Huvenne, T. P. Le Bas et al., "Autonomous Underwater Vehicles (AUVs): their past, present and future contributions to the advancement of marine geoscience," *Marine Geology*, vol. 352, pp. 451–468, 2014.

[10] G. R. L. Tu, X. Xu, K. Watanabe, and I. Nagai, "Stabilizing control for the attitude of a small-sized X4-AUV," in *Proceedings of the 55th Annual Conference of the Society of Instrument and Control Engineers of Japan, SICE 2016*, pp. 1185–1190, September 2016.

[11] N. Harun, Z. M. Zain, and M. M. Noh, "PSO approach for a PID back-stepping control method in stabilizing an underactuated X4-AUV," in *Proceedings of the 7th IEEE International Conference on Underwater System Technology: Theory and Applications, USYS 2017*, pp. 1–6, Malaysia, December 2017.

[12] K. Watanabe, S. Takisawa, and I. Nagai, "Underactuated control for an X4-AUV using partial linearization and attitude linearization," in *Proceedings of the 2013 13th International Conference on Control, Automation and Systems, ICCAS 2013*, pp. 1425–1430, Republic of Korea, October 2013.

[13] Z. M. Zain, M. M. Noh, K. A. Ab Rahim, and N. Harun, "Design and development of an X4-ROV," in *Proceedings of the 6th IEEE International Conference on Underwater System Technology: Theory and Applications, USYS 2016*, pp. 207–211, December 2016.

[14] G. R. L. Tu, K. Watanabe, and I. Nagai, "The design and production of thrusters for an AUV without rudders," in *Proceedings of the 10th Asian Control Conference, ASCC 2015*, pp. 1–4, June 2015.

[15] Z. M. Zain, N. Harun, K. Watanabe, and I. Nagai, "Comparison of an X4-AUV performance using a direct Lyapunov - PD controller and backstepping approach," in *Proceedings of the 10th Asian Control Conference, ASCC 2015*, pp. 1–6, June 2015.

[16] R. Zheng, Y. Ma, B. Zhang et al., "Stable control for AUV's near-bottom and low-speed sailing based on vertical thruster," *Jiqiren/Robot*, vol. 38, no. 5, pp. 588–592, 2016.

[17] L. V. Steenson, A. B. Phillips, E. Rogers et al., "Control of an AUV from thruster actuated hover to control surface actuated flight," *Specialists Meeting Avt-189/rsm-028 Assessment of Stability & Control Prediction Methods for Nato Air & Sea Vehicles*, 2011.

[18] A. Saunders and M. Nahon, "The effect of vehicle velocity and drift angle on through-body AUV tunnel thruster performance," *Ocean Systems Engineering*, vol. 1, no. 4, pp. 297–315, 2011.

[19] L. G. Miller and K. V. Ellenrieder, "Modeling and simulation of an AUV-towfish system," in *Proceedings of the OCEANS 2013 MTS/IEEE San Diego Conference: An Ocean in Common*, September 2014.

[20] M. T. Issac, S. Adams, N. Bose, C. D. Williams, R. Bachmayer, and T. Crees, "Analysis of horizontal zigzag manoeuvring trials from the MUN explorer AUV," in *Proceedings of the OCEANS 2008*, pp. 1–7, September 2008.

[21] L. V. Steenson, A. B. Phillips, M. Furlong et al., "Maneuvering of an over-actuated autonomous underwater vehicle using both through-body tunnel thrusters and control surfaces," *Autonomous Underwtaer Vehicles Applications Center*, 2011.

[22] K. Kim, J. Kim, H. S. Choi, K.-Y. Lee, and W. Seong, "Estimation of hydrodynamic coefficients of a test-bed AUV-SNUUV I by motion test," in *Proceedings of the Ocean's 2002 Conference and Exhibition*, pp. 186–190, USA, October 2002.

[23] J. Dantas and E. d. Barros, "Numerical analysis of control surface effects on AUV manoeuvrability," *Applied Ocean Research*, vol. 42, pp. 168–181, 2013.

[24] G. da Silva Costa, A. Ruiz, M. Reis et al., "Numerical analysis of stability and manoeuvrability of Autonomous Underwater Vehicles (AUV) with fishtail shape," *Ocean Engineering*, vol. 144, pp. 320–326, 2017.

[25] T. Fossen, *Handbook of Marine Craft Hydrodynamics and Motion Control*, John Wiley & Sons Ltd., UK, 2011.

[26] W. Xiaoming, *Dynamical behavior and control strategies of the Hybrid Autonomous Underwater Vehicle*, Tianjin University, Tianjin, China, 2009.

[27] A. Mofidi and P. M. Carrica, "Simulations of zigzag maneuvers for a container ship with direct moving rudder and propeller," *Computers & Fluids*, vol. 96, pp. 191–203, 2014.

[28] J. Wang, L. Zou, and D. Wan, "Numerical simulations of zigzag maneuver of free running ship in waves by RANS-Overset grid method," *Ocean Engineering*, vol. 162, pp. 55–79, 2018.

[29] P. M. Carrica, A. Mofidi, K. Eloot et al., "Direct simulation and experimental study of zigzag maneuver of KCS in shallow water," *Ocean Engineering*, vol. 112, pp. 117–133, 2016.

[30] X. Liang, Y. Li, Z. Peng et al., "Nonlinear dynamics modeling and performance prediction for underactuated AUV with fins," *Nonlinear Dynamics*, vol. 84, no. 1, pp. 237–249, 2016.

[31] D. Fei and P. Shuo, "Motion simulation based on the modified REMUS model," *Applied Science and Technology*, vol. 39, no. 4, pp. 83–88, 2012.